Biochemistry

 Volume 38, Number 38 September 21, 1999

Accelerated Publications

Mössbauer Studies of the Formation and Reactivity of a Quasi-Stable Peroxo Intermediate of Stearoyl-Acyl Carrier Protein Δ^9-Desaturase†

John A. Broadwater,‡ Catalina Achim,§ Eckard Münck,*,§ and Brian G. Fox*,‡

The Institute for Enzyme Research, Graduate School, University of Wisconsin, Madison, Wisconsin 53705, Department of Biochemistry, College of Agricultural and Life Sciences, University of Wisconsin, Madison, Wisconsin 53706, and Department of Chemistry, Carnegie Mellon University, Pittsburgh, Pennsylvania 15217

Received June 21, 1999; Revised Manuscript Received August 6, 1999

ABSTRACT: Stearoyl-ACP Δ^9-desaturase (Δ9D) is a diiron enzyme that catalyzes 18:0-ACP desaturation. Each subunit of homodimeric resting Δ9D contains a diferric cluster, while chemical reduction by $4e^-$ produces a diferrous cluster in each subunit. Reaction of $4e^-$-reduced Δ9D with 18:0-ACP and O_2 yields a blue chromophore ($\lambda_{max} \sim 700$ nm) that exhibits a vibrational spectrum indicative of a μ-1,2-peroxo complex; this species has been designated peroxoΔ9D. In contrast to other enzymic peroxodiiron intermediates, peroxoΔ9D is long-lived ($t_{1/2} \sim 30$ min at 25 °C) and decays via an oxidase reaction without formation of either H_2O_2 or product (18:1-ACP). In this work, optical, transient kinetic, and Mössbauer techniques have been used to further investigate the origin and nature of this unusual peroxodiiron complex. Rapid mixing of $4e^-$ Δ9D with O_2-equilibrated 18:0-ACP produced peroxoΔ9D as revealed by a temperature-dependent, pseudo-first-order absorption increase at 700 nm ($k = 46$ s^{-1} at 6 °C). The Mössbauer spectrum of peroxoΔ9D, accounting for 96% of the total iron, consists of two quadrupole doublets present in equal proportions: $\delta(1) = 0.68(1)$ mm/s, and $\Delta E_Q(1) = 1.90(2)$ mm/s; $\delta(2) = 0.64(1)$ mm/s, and $\Delta E_Q(2) = 1.06(2)$ mm/s. Decay of the 700 nm optical band ($k = 0.004$ min^{-1} at 6 °C) correlates with the complete conversion of peroxoΔ9D into a complex called peroxo-cycled Δ9D, which exhibits two new doublets present in equal proportions: $\delta(1) = 0.57(2)$ mm/s, and $\Delta E_Q(1) = 1.91(3)$ mm/s; $\delta(2) = 0.52(2)$ mm/s, and $\Delta E_Q(2) = 1.41(3)$ mm/s. Thus, peroxoΔ9D contains two asymmetric diferric clusters and reacts to yield peroxo-cycled Δ9D, also containing two asymmetric diferric clusters that most probably represent a substrate complex state. The clusters of both peroxoΔ9D and peroxo-cycled Δ9D have a diamagnetic ground state. Because peroxoΔ9D and peroxo-cycled Δ9D are observed only in the presence of 18:0-ACP, substrate binding appears to have introduced asymmetry into the Δ9D diiron clusters. In situ photolysis of peroxoΔ9D at 4.2 K in the Mössbauer cryostat caused the release of O_2 and the reappearance of a diferrous Δ9D·18:0-ACP complex with slightly changed parameters, suggesting a constrained cluster configuration was produced by the photolysis event. Annealing the photolyzed sample for 30 min at 77 K quantitatively restored the Mössbauer spectrum of peroxoΔ9D, showing that the released O_2 was effectively sequestered within the active site.

Enzymes containing diiron sites are a functionally and structurally diverse group (*1*, *2*). Among these, RNR R2[1] (*3*), bacterial hydrocarbon monooxygenases (*4*), acyl-ACP desaturases (*5*), ferritins (*6*), and rubrerythrins (*2*) catalyze O_2 activation as part of their alternative catalytic cycles. Studies of these enzymes have revealed a rich variety of

10.1021/bi9914199 CCC: $18.00
Published on Web 09/03/1999

cluster redox states, including diferric (*7*−*10*), diferrous (*8*, *11*−*16*), μ-1,2-peroxo (*17*−*24*), ferric−ferryl (*25*−*28*), and diferryl (*22*, *24*, *29*). Two important goals of these research efforts are to establish whether similar reactive intermediates are produced by all of these different enzymes and, if so, to determine how each enzyme modulates the respective intermediates to perform their unique catalytic tasks.

Stearoyl-ACP Δ^9-desaturase (Δ9D) is the best characterized acyl-ACP desaturase (*5*). This soluble, homodimeric enzyme ($M_r \approx 84$ kDa) catalyzes the NAD(P)H- and O_2-dependent introduction of a cis double bond between carbons 9 and 10 of stearoyl-ACP (18:0-ACP, ~9 kDa) to yield oleoyl-ACP (18:1-ACP) with a turnover number of 0.3−0.5 s^{-1}. Optical, Mössbauer, resonance Raman, and EXAFS studies (*30*−*32*) have shown that resting Δ9D contains two oxo- or hydroxo-bridged diferric centers, while the X-ray structure of the photoreduced enzyme (containing two diferrous clusters) revealed that a diiron center is buried within each subunit (*33*). A prominent tunnel, proposed to be the substrate binding site, starts at the surface of each subunit, bends at the diiron center, and then continues almost entirely through the enzyme. MCD studies showed that the two diferrous clusters of 4e$^-$ Δ9D contain two equivalent five-coordinate Fe sites with distorted square pyramidal geometries, consistent with the ~2.4 Å X-ray structure, while the addition of 18:0-ACP changed one Fe site of each cluster to a four-coordinate distorted tetrahedral geometry and caused substantial changes in the ground and excited state electronic structure (*13*). The latter MCD studies provided the first structural evidence for a potential role of 18:0-ACP binding in the O_2 activation step(s) required for Δ9D catalysis.

Rapid-freeze Mössbauer studies of the peroxo intermediates of MMOH, RNR R2, and ferritin have revealed a single, quadrupole doublet [$\delta \approx 0.62-0.66$ mm/s and $\Delta E_Q \approx 1.08-1.58$ mm/s (*17*, *19*, *22*, *23*)], indicating that the two Fe atoms in these diamagnetic complexes are in the ferric state and have similar coordination environments. Moreover, optical and resonance Raman studies with intermediates obtained from the reaction of O_2 with the W48F/D84E isoform of RNR R2, ferritin, and the 18:0-ACP complex of 4e$^-$ Δ9D have revealed a blue chromophore ($\lambda_{max} \approx 700$ nm) with ν(O−O) frequencies (851−898 cm^{-1}) and spectral patterns in the $^{16}O^{18}O$ complex that are consistent with a μ-1,2-peroxo coordination geometry (*18*, *20*, *21*). However, among these complexes, peroxoΔ9D exhibits remarkable stability ($t_{1/2}$ ~ 30 min for the loss of the 700 nm optical band at 25 °C) and then decays by an oxidase reaction without release of H_2O_2 and without formation of desaturated product (*18*). In the work presented here, optical, transient kinetic, and Mössbauer techniques have been used to further investigate the origin and nature of peroxoΔ9D. These studies reveal that 18:0-ACP binding has substantial influence on both the diferric and the diferrous clusters of Δ9D, that addition of O_2 to the complex of 18:0-ACP and 4e$^-$ Δ9D leads to peroxoΔ9D, which contains diiron clusters with spectroscopically distinguishable iron sites, and that peroxoΔ9D can be reversibly photodissociated to produce O_2 and diferrous clusters.

MATERIALS AND METHODS

Enzyme Preparation. Δ9D from *Ricinus communis* was overexpressed in *Escherichia coli* BL21(DE3) (*34*). For ^{57}Fe enrichment, a 500 mL starting inoculum was grown in M9 minimal medium supplemented with 5 μM $^{56}FeSO_4$ to an optical density at 600 nm of ~0.7. This inoculum was transferred to 5 L of M9 medium contained in a New Brunswick Bioflow 3000 fermenter. The fermenter medium was supplemented with 10 g of Casamino acids (Difco, Detroit, MI), 35 g of glucose, and 6 mg of ^{57}Fe metal (95% isotopic enrichment, Pennwood Chemicals) dissolved in 2 M HCl. During cell growth, the dissolved O_2 was maintained at 30% of saturation by feedback control of the agitation rate and the pH was maintained at 7.0 ± 0.1 by controlled addition of 4 M NH_4OH. Cells were induced at an optical density at 600 nm of ~9 by the rapid addition of 25 g of β-D-lactose. At induction, the culture was supplemented with 23 mg of ^{57}Fe metal dissolved in 2 M HCl (final concentration of 80 μM). The culture was harvested after 3.5 h by centrifugation. Resting [^{57}Fe]Δ9D was purified, concentrated, quantitated, and assayed as previously described (*34*, *35*); 18:0-ACP was prepared as previously described (*35*).

Stopped-Flow Spectroscopy. Stopped-flow experiments were performed using an OLIS stopped-flow device and rapid-scanning monochromator (Bogart, GA). The ram syringes, mixer, and optical cell were maintained at the desired temperature by using a refrigerated water bath and a methanol/water mixture. Reactions were initiated by rapidly mixing equal volumes of 4e$^-$ Δ9D (200 μM holoprotein) and 18:0-ACP (400 μM). To maximize the formation of peroxoΔ9D, the 18:0-ACP solution was equilibrated with 1 atm of O_2 prior to mixing. Absorbance spectra were recorded either from 560 to 780 nm or from 310 to 440 nm at a sampling rate of 1000 scans/s. The absorbance intensity data were best fit by a single exponential with correction for initial absorbance background $\{a(t) = a(\infty)[1 - \exp(-kt)]\}$.

Samples for Spectroscopic Studies. 4e$^-$ Δ9D was prepared as previously described (*18*, *31*); oxygenated 4e$^-$ Δ9D was prepared by flushing the optical cuvette with O_2 after reduction. [^{57}Fe]PeroxoΔ9D was prepared by adding 18:0-ACP to oxygenated 4e$^-$ Δ9D in a septum-sealed optical cuvette (*18*). Decay of peroxoΔ9D was monitored from 300 to 800 nm using a Hewlett-Packard 8452A diode array spectrophotometer. For the correlation of absorbance and Mössbauer measurements, 250 μL aliquots of ^{57}Fe-enriched peroxoΔ9D were transferred from the optical cuvette to a Mössbauer sample cup at appropriate time points during the

† This work was supported by the National Institutes of Health (Grant GM-50853 to B.G.F. and Grant GM-22701 to E.M.). B.G.F. is a Shaw Scientist of the Milwaukee Foundation (1994−1999). J.A.B. is a trainee being supported by NIH Institutional Molecular Biophysics Pre-Doctoral Training Grant T32 GM-08293.

* To whom correspondence should be addressed. B.G.F.: e-mail, fox@enzyme.wisc.edu; telephone, (608) 262-9708. E.M.: e-mail, em40@andrew.cmu.edu; telephone, (412) 268-5058.

‡ University of Wisconsin.

§ Carnegie Mellon University.

[1] Abbreviations: ACP, recombinant acyl carrier protein containing a C-terminal His_6 sequence; 18:0-ACP, stearoyl-ACP; 18:1-ACP, oleoyl-ACP; Δ9D, 18:0-ACP Δ^9-desaturase; resting Δ9D, as-isolated form of Δ9D containing two diferric clusters; 4e$^-$ Δ9D, chemically reduced form of Δ9D containing two diferrous clusters; peroxoΔ9D, form of Δ9D containing two μ-1,2-peroxo clusters; peroxo-cycled Δ9D, form of Δ9D obtained from decay of peroxoΔ9D; MMOH, hydroxylase component of methane monooxygenase; compound P, peroxo intermediate of MMOH; RNR R2, iron-containing component of ribonucleotide diphosphate reductase.

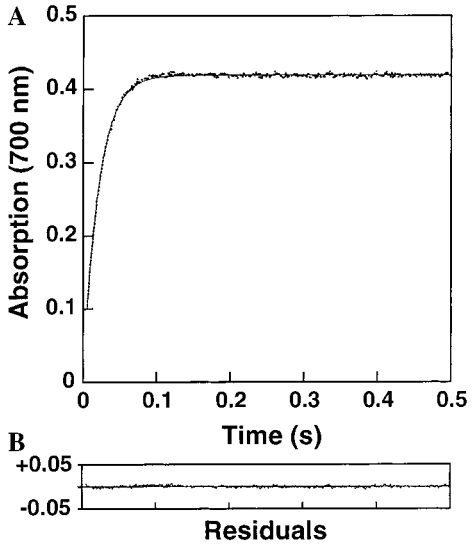

FIGURE 1: Intensity changes for the 700 nm optical band of peroxoΔ9D at 6 °C. (A) Data (dotted line) were best fit by a pseudo-first-order single-exponential with a k of 46 s^{-1}. (B) Residual errors for the nonlinear least-squares fit.

decay reaction and quickly frozen with liquid N_2. The time-dependent changes in the intensity of the absorbance and Mössbauer spectra were simulated using the Levenberg−Marquardt nonlinear least-squares fitting routines provided in Mathematica 2.2 (Wolfram Research, Inc., Champaign, IL). These data were best fit by $a(t) = a(\infty) + a(0)\exp(-kt)$ for intensities that decreased over time and $a(t) = a(\infty)[1 - \exp(-kt)]$ for intensities that increased over time.

Mössbauer Spectroscopy. Spectra were obtained on constant-acceleration instruments, and isomeric shifts are reported relative to an Fe metal standard at room temperature. Spectral simulations were generated using WMOSS [WEB Research, Edina, MN (*9*)]. For photolysis experiments in the Mössbauer dewar, Δ9D (1.1 mM) and 18:0-ACP (2.4 mM) were prepared in 50% (v/v) glycerol prior to reduction to create a glass upon freezing. After reduction, the sample cuvette was filled with O_2 to form peroxoΔ9D. Photolysis experiments were performed using white light from a 300 W projection lamp bulb. The light beam was focused by a water-filled round-bottom flask (10 cm diameter) and collimated by a leucite cone into a leucite light pipe that guided the light beam to the sample. The glassed sample was maintained at 4.2 K and exposed to light for 1 h prior to Mössbauer data collection. After the initial data collection, the sample was reirradiated for 1 h and another set of data was collected. Following data collection, the sample was warmed to 77 K for 30 min to allow O_2 rebinding.

RESULTS

Optical Detection of the Formation and Decay of PeroxoΔ9D. In a previous resonance Raman study, we suggested that an optical band at 700 nm is associated with a μ-1,2-peroxodiferric species called peroxoΔ9D (*18*). Rapid mixing of 4e$^-$ Δ9D with O_2-equilibrated 18:0-ACP gave a single-exponential increase in absorption with the same rate constant when monitored at either 700 nm (Figure 1) or 350 nm (data not shown). The pseudo-first-order formation rate (k) for peroxoΔ9D was temperature-dependent, increasing from 46 s^{-1} at 6 °C to 87 s^{-1} at 24 °C. A single-exponential fit of a quality comparable to that shown in Figure 1 was obtained at each temperature that was examined. At 24 °C, the formation reaction was complete within less than 200 ms, and because of subsequent slow decay (see below), less than 3% spectral change was observed after 1 min. The decay was also best fit as a temperature-dependent, single-exponential process with a decrease in rate k from 0.06 min^{-1} at 30 °C to 0.004 min^{-1} at 6 °C (a representative fit for the decay at 20 °C is shown in Figure 3B of ref *18*). The $\Delta H^{\ddagger}$ and $\Delta S^{\ddagger}$ values derived from Eyring plots for the formation and decay reactions are provided in Table 1.

Table 1: Thermodynamic Parameters[a] for Various Peroxodiiron Complexes

complex	$\Delta H^{\ddagger}$ (kJ mol^{-1})[b]	$\Delta S^{\ddagger}$ (J mol^{-1} K^{-1})[c]	ref
formation reactions			
peroxoΔ9D	22	−134	this work
[$Fe_2(\mu$-1,2-O_2)(HMTMP)]	39−42	−65 to −114	*45*
[$Fe_2(\mu$-1,2-O_2)(HPTP)]	16	−114	*45*
[$Fe_2(\mu$-1,2-O_2)(Et-HPTB)]	15	−121	*45*
oxyhemerythrin	17	−46	*46*
MMOH compound P, C_2H_2	92	88	*24*
decay reactions			
peroxoΔ9D	80	−41	this work
[$Fe_2(\mu$-1,2-O_2)(HPTP)]	52	−47	*45*
[$Fe_2(\mu$-1,2-O_2)(Et-HPTB)]	65	−46	*38*
oxyhemerythrin	70	38	*46*
[$Fe_2(\mu$-1,2-O_2)(Et-HPTB)]	81	74	*45*
MMOH compound P, CH_4	168	140	*47*
MMOH compound P	114	163	*24*

[a] Calculated from the Eyring equation, $\ln(kh/k_BT) = \Delta S^{\ddagger}/R - \Delta H^{\ddagger}/RT$, where k is the observed rate and the other variables and constants have the standard meanings. The rates of formation and decay of peroxoΔ9D were determined from 6 to 30 °C. For the formation reaction, the r^2 value from least-squares fitting was 0.9954. For the decay reaction, the r^2 value was 0.9963. [b] Slope of the Eyring plot. [c] Intercept of the Eyring plot.

Mössbauer Detection of the Formation and Decay of PeroxoΔ9D. The Mössbauer spectrum of 4e$^-$ Δ9D, shown in Figure 2A, consists of a superposition of two (unresolved) doublets: $\delta(1) \approx 1.27$ mm/s, and $\Delta E_Q(1) \approx 3.30$ mm/s; $\delta(2) \approx 1.28$ mm/s, and $\Delta E_Q(2) \approx 3.05$ mm/s (Table 2). These parameters are characteristic of high-spin ferrous sites in octahedral oxygen−nitrogen environments. Addition of 18:0-ACP to an anaerobic sample of 4e$^-$ Δ9D caused a slight broadening of these doublets, but otherwise, no major changes were detected in the parameters of the zero-field spectrum. No absorption bands were detected in the optical spectrum of anaerobic 4e$^-$ Δ9D, either in the absence or in the presence of 18:0-ACP (see Figure 1 of ref *18*).

Figure 2B and Figure 3A (solid line) show the Mössbauer and optical spectra of a sample frozen 1 min after the complex of ^{57}Fe-enriched 4e$^-$ Δ9D and a 2-fold excess of 18:0-ACP was mixed with O_2. In the Mössbauer spectrum, 96% of the doublet of 4e$^-$ Δ9D (Figure 2A) was replaced by two new doublets (Table 2 and Figure 2B). The four absorption lines in Figure 2B can be grouped into two doublets in two different ways. Counting from the left, one can assign lines 1 and 4 and lines 2 and 3 as doublets, or alternatively, lines 1 and 3 and lines 2 and 4 can be assigned as doublets. The latter association would yield, in our view, to unreasonable isomer shifts for the two sites [$\delta(1) = 0.87$ mm/s and $\delta(2) = 0.45$ mm/s]. We therefore conclude that peroxoΔ9D consists of two doublets representing 96% of

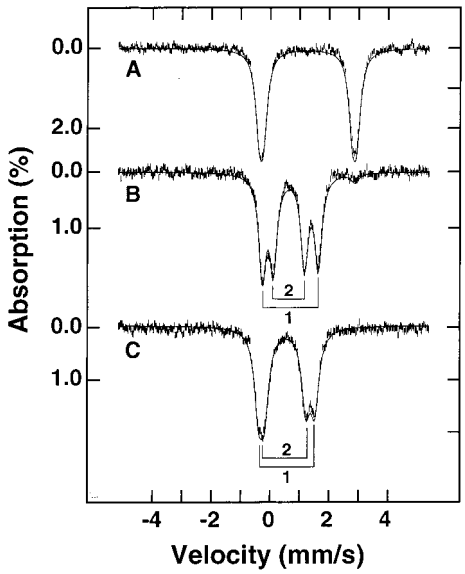

FIGURE 2: Mössbauer spectra of diiron species produced during the formation and decay of peroxoΔ9D. (A) 4e⁻ Δ9D (∼250 μM homodimers, 3.8 mol of Fe per mole of homodimer). (B) PeroxoΔ9D obtained 1 min after mixing 4e⁻ Δ9D, 18:0-ACP, and O_2. (C) Peroxo-cycled Δ9D obtained after decay of peroxoΔ9D. Solid lines are spectral simulations using the parameters listed in Table 2. Brackets indicate the association of absorption lines.

Table 2: Mössbauer Parameters Observed during the Reaction of the Complex of 4e⁻ Δ9D and 18:0-ACP with O_2

sample		δ (mm/s)	ΔE_Q (mm/s)	percentage
resting Δ9D[a]		0.54	1.53	72
		0.49	0.72	21
		0.50	2.20	7
peroxoΔ9D[b] ($S = 0$)	site 1	0.68(1)	1.90(2)	48
	site 2	0.64(1)	1.06(2)	48
peroxo-cycled Δ9D[c] ($S = 0$)	site 1	0.57(2)	1.91(3)	48
	site 2	0.52(2)	1.41(3)	48
4e⁻ Δ9D (diferrous)[d] and substrate complex	site 1	≈1.27	≈3.30	50
	site 2	≈1.28	≈3.05	50
diferrous after photolysis	site 1	≈1.24	≈3.20	50
	site 2	≈1.20	≈2.80	50

[a] Diferric enzyme obtained from the standard purification procedure as characterized by Mössbauer spectroscopy (*32*). [b] Peroxo-level intermediate obtained by reaction of 4e⁻ Δ9D with 18:0-ACP and O_2. [c] Diferric state obtained by decay of peroxoΔ9D. [d] Diferrous state of Δ9D obtained by methyl viologen-mediated 4e⁻ reduction with sodium dithionite and the 18:0-ACP complex of 4e⁻ Δ9D.

the total Fe with the following parameters: $\delta(1) = 0.68(1)$ mm/s, and $\Delta E_Q(1) = 1.90(2)$ mm/s; $\delta(2) = 0.64(1)$ mm/s, and $\Delta E_Q(2) = 1.06(2)$ mm/s. Mössbauer spectra recorded in applied fields up to 8.0 T (not shown) revealed that peroxoΔ9D has a diamagnetic electronic ground state, and thus, peroxoΔ9D contains diiron clusters with two distinct iron sites.

Examination of the optical and Mössbauer spectra of samples prepared 18, 44, and 94 min after the addition of O_2 showed that the decrease in the intensity of the 700 nm optical band is accompanied by a decrease in the intensity of the Mössbauer spectrum assigned to peroxoΔ9D and the appearance of a new pair of doublets: $\delta(1) = 0.57(2)$ mm/s, and $\Delta E_Q(1) = 1.91(3)$ mm/s; $\delta(2) = 0.52(2)$ mm/s, and $\Delta E_Q(2) = 1.41(3)$ mm/s. For a sample frozen 94 min after the addition of O_2 [Figures 2C and 3A (dotted line)], the new doublets represent all the iron initially contained in

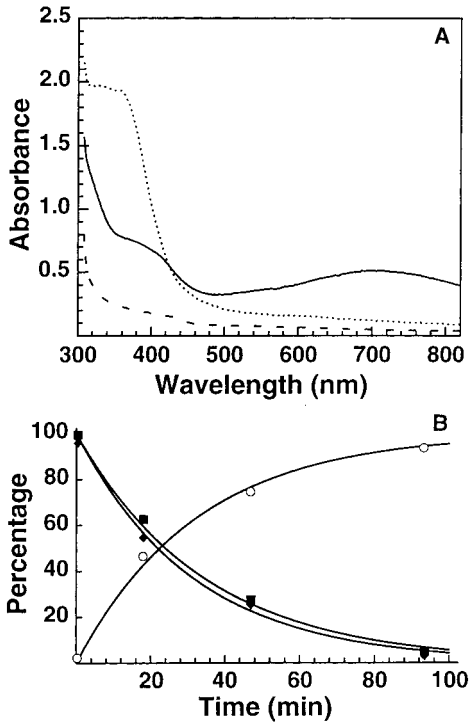

FIGURE 3: (A) Optical spectra of the Mössbauer samples used to produce the data depicted in Figure 2: (—) sample from Figure 2B (peroxoΔ9D), (···) sample from Figure 2C (peroxo-cycled Δ9D), and (- - -) sample described in footnote 4. (B) Disappearance of the 700 nm optical band (■) and Mössbauer spectrum (◆) of peroxoΔ9D and the appearance of peroxo-cycled Δ9D (○) in a sample incubated at 24 °C. The solid lines are least-squares fits based on single-exponential decreases in the intensities of the optical and Mössbauer spectra of peroxoΔ9D, and a single-exponential increase in the intensity of the Mössbauer spectrum of peroxo-cycled Δ9D.

peroxoΔ9D (96%). After the sample used to produce the data depicted in Figure 2C was thawed and allowed to stand for 15 h at 25 °C, the Mössbauer spectrum was found to be unchanged. Thus, the doublets of Figure 2C represent clusters with distinguishable iron sites in a stable state of the enzyme, which we call peroxo-cycled Δ9D. A Mössbauer spectrum taken in an 8.0 T applied magnetic field (not shown) revealed that peroxo-cycled Δ9D is diamagnetic, while the optical spectrum [Figure 3A (dotted line)] is consistent with the presence of an oxo-bridged diferric cluster. The difference in the Mössbauer parameters between peroxo-cycled and resting Δ9D suggested that the spectrum of Figure 2C might represent the complex of resting Δ9D with 18:0-ACP. Indeed, subsequent experiments showed that the addition of excess 18:0-ACP to resting Δ9D yielded a Mössbauer spectrum (data not shown) consistent with a superposition of the spectra of peroxo-cycled Δ9D (∼70%) and resting Δ9D. This observation suggests that Figure 2C represents a stoichiometrically formed complex of resting Δ9D with 2 mol of 18:0-ACP.[2]

[2] Resonance Raman studies with peroxo-cycled Δ9D revealed ∼5 and ∼13 cm^{-1} shifts in ν_s(Fe−O) and ν_{as}(Fe−O), respectively, relative to those of resting Δ9D. Titration of 18:0-ACP into resting Δ9D produced frequency shifts similar to those observed with peroxo-cycled Δ9D, but the binding affinity for complex formation with resting Δ9D was considerably weaker than that for complex formation with 4e⁻ Δ9D (K. S. Lyle, J. Ai, T. M. Loehr, J. Sanders-Loehr, and B. G. Fox, unpublished results).

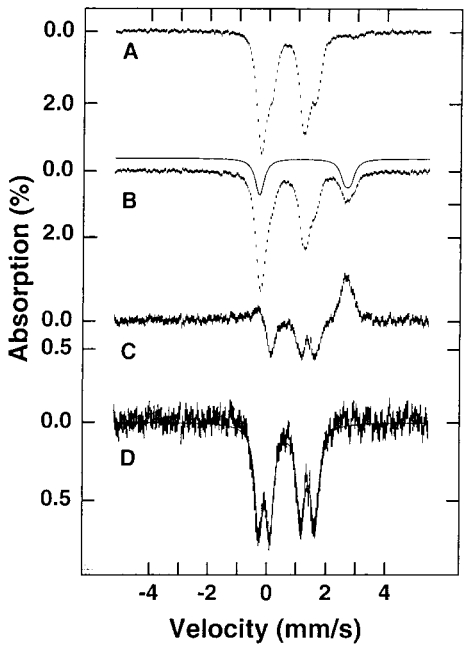

FIGURE 4: Conversion of peroxoΔ9D into a diferrous cluster upon photolysis. (A) PeroxoΔ9D before illumination. (B) PeroxoΔ9D after illumination for 1 h at 4.2 K. The solid line above the data is a spectral simulation for two ferrous quadrupole doublets with equal intensity using the parameters listed in Table 2. (C) B minus A difference spectrum. (D) C minus the simulated spectrum in B difference spectrum. The solid line is a simulation for two quadrupole doublets with equal intensity having the parameters listed in Table 2 for peroxoΔ9D.

Due to partial spectral overlap of peroxoΔ9D and peroxo-cycled Δ9D, it was initially not obvious whether the two doublets shown in parts B and C of Figure 2 would represent one cluster with distinct iron sites or two distinct clusters with similar iron sites. However, we were able to resolve this question with a low-temperature photolysis study.

Low-Temperature Photolysis Reaction. Figure 4A shows a 4.2 K Mössbauer spectrum of peroxoΔ9D prepared in a 50:50 (v/v) buffer/glycerol solution. Notably, only a trace amount (≈3%) of diferrous cluster is present. A detailed analysis of the spectrum of Figure 4A (see below) shows that 60% of the total iron belongs to peroxoΔ9D, while the remainder belongs to a doublet structure with an average isomer shift δ of ≈0.5 mm/s.[3] Figure 4B shows a spectrum recorded at 4.2 K after the sample was illuminated in situ for 1 h at 4.2 K. Comparison of parts B and A of Figure 4 shows that illumination led to a substantial increase in the proportion of diferrous cluster and a substantial decrease in the intensity of the peroxoΔ9D absorption. Figure 4C shows a difference spectrum obtained by subtracting the "dark" spectrum (Figure 4A) from the spectrum of the illuminated sample (Figure 4B). The spectrum shown in Figure 4D was obtained by subtracting the diferrous contribution (simulated spectrum drawn above the data of Figure 4B; see below) from Figure 4C. Therefore, Figure 4D represents the spectral components that disappear upon illumination. This spectrum consists of two doublets with equal intensity, and moreover, the observed parameters are identical to those assigned to peroxoΔ9D. The photolysis data thus establish that both doublets of Figure 2B belong to a single cluster type in peroxoΔ9D, and confirm that 96% of the diiron clusters in the sample of Figure 2B are a peroxo complex formed in the presence of 18:0-ACP.

We now comment briefly on the spectral simulations presented in Figure 4. The positions of the three high-energy lines of the two doublets shown in Figure 4D are well-defined in the difference spectrum of Figure 4C. However, the contributions of the low-energy lines of doublet 1 (see Figure 2B) and the diferrous cluster produced by photolysis cancel in the difference spectrum. Comparison of Figure 2B and Figure 4D shows that the positions of the three higher-energy lines of peroxoΔ9D are unchanged in samples prepared either with or without glycerol. It is thus reasonable to assume that the position of the fourth, lower-energy line is also independent of the presence of glycerol. With this assumption, the positions of the low-energy lines of the two doublets of the diferrous cluster produced by photolysis are established. The solid line drawn above the spectrum of Figure 4B is a spectral simulation of the diferrous cluster; the spectrum is best described by a superposition of two ferrous doublets: $\delta(1) \approx 1.24$ mm/s, and $\Delta E_Q(1) \approx 3.20$ mm/s; $\delta(2) \approx 1.20$ mm/s, and $\Delta E_Q(2) \approx 2.80$ mm/s (Table 2). Thus, photolysis released O_2 from peroxoΔ9D, and yielded a diferrous state measurably different from the 4e$^-$ Δ9D·18:0 ACP complex used to produce peroxoΔ9D.

For the photolyzed sample used to produce the data depicted in Figure 4B, no measurable rebinding of O_2 was observed at 4.2 K over a period of 12 h. After the spectrum depicted in Figure 4B had been collected, the sample was warmed to 77 K in the Mössbauer dewar, kept at 77 K for 30 min, and then cooled to 4.2 K. The spectrum subsequently collected at 4.2 K was essentially identical to that depicted in Figure 4A, showing that O_2 had rebound to the diferrous center to quantitatively reform peroxoΔ9D. To test the wavelengths that were most efficient for photolysis, the sample was illuminated for 1 h through a long-path filter (cut-on wavelength of 645 nm); this produced the same result that was obtained without the filter, suggesting that illumination in the 700 nm optical band is sufficient for photolysis.

Correlation of Optical and Mössbauer Results. After the positions of all the lines of parts B and C of Figure 2 had been established, the time dependence of the changes in the optical and Mössbauer spectra during the decay of peroxoΔ9D to peroxo-cycled Δ9D could be readily determined. Figure 3B shows that the changes in intensity of both the optical and the Mössbauer spectra can be fit with a single-exponential constant ($k = 0.031 \pm 0.002$ min^{-1}) at 24 °C. This value agrees well with that determined previously at 20 °C by optical spectroscopy alone (*18*). By using the Mössbauer results of Figure 2, which show essentially quantitative formation of peroxoΔ9D and peroxo-cycled Δ9D, and the protein and Fe concentrations determined by colorimetric methods, ϵ values per diiron cluster were

[3] A fraction of material with a δ of ≈0.5 mm/s (∼40%) appears to be resting Δ9D that was not reduced, possibly due to difficulties in mixing and equilibrating the 50% (v/v) glycerol sample. Thus, the sample contained 60% peroxoΔ9D, 3% 4e$^-$ Δ9D, and 37% resting Δ9D.

[4] A small, reproducible rise in the absorption at ∼350 nm was observed upon mixing 4e$^-$ Δ9D with O_2 in the absence of 18:0-ACP (dashed line in Figure 3B). The identity of this species is not known, and its spectral contribution was subtracted before the molar absorptivity values were calculated.

determined for peroxoΔ9D at 700 nm ($\epsilon = 1100 \pm 80$ M^{-1} cm^{-1}) and 350 nm ($\epsilon = 1100 \pm 80$ M^{-1} cm^{-1}) and for peroxo-cycled Δ9D at 340 nm ($\epsilon = 4850 \pm 375$ M^{-1} cm^{-1}).[4]

DISCUSSION

Kinetics and Temperature Dependence. The rate of the reaction between $4e^-$ Δ9D, 18:0-ACP, and O_2 (~87 s^{-1} at 24 °C) is comparable to the rates for the analogous reactions of diferrous MMOH, RNR R2, and ferritin, and would apparently be competent to initiate the Δ9D desaturase reaction (0.3−0.5 s^{-1} at 25 °C). Yet, peroxoΔ9D is remarkably long-lived and does not progress to desaturation catalysis. Table 1 shows that the $\Delta H^{\ddagger}$ and $\Delta S^{\ddagger}$ values for formation and decay of peroxoΔ9D and certain synthetic μ-1,2-peroxodiferric model complexes are similar, but differ substantially from the values for the η^1-peroxo complex of oxyhemerythrin ($\Delta S^{\ddagger}$ values) and for MMOH compound P (both $\Delta H^{\ddagger}$ and $\Delta S^{\ddagger}$ values). For peroxoΔ9D and oxyhemerythrin, the difference in the $\Delta S^{\ddagger}$ values for formation and decay may reflect a more ordered transition state that is required for formation of a μ-1,2- versus an η^1-peroxo complex. The large differences in both the $\Delta H^{\ddagger}$ and $\Delta S^{\ddagger}$ values of peroxoΔ9D and MMOH compound P, which are both proposed to form μ-1,2 complexes, are more difficult to rationalize, but may arise from differences in the chemical reactivities of these intermediates or from the complexity of other protein−protein or protein−substrate interactions that are required for the enzyme reactions.

Mössbauer Properties of PeroxoΔ9D. The high-spin ferric sites of diiron clusters have δ values ranging from 0.45 to 0.55 mm/s. Shifts above 0.60 mm/s, up to 0.66 mm/s, have been reported for peroxoferric complexes (*17*, *19*, *22*, *23*, *36*−*38*). Recently, Bollinger et al. (*17*) have characterized a peroxo complex of the D84E isoform of *E. coli* RNR R2; in the native enzyme, D84 coordinates in a bidentate fashion to one Fe of the diiron cluster (*3*). The peroxo complex of D84E RNR R2 exhibits a single quadrupole doublet: $\delta = 0.63$ mm/s, and $\Delta E_Q = 1.58$ mm/s. Likewise, MMOH compound P exhibits a single quadrupole doublet: $\delta = 0.66$ mm/s, and $\Delta E_Q = 1.51$ mm/s (*22*, *23*). On average, the $\delta(1)$ value of 0.68 mm/s and the $\delta(2)$ value of 0.64 mm/s observed for the inequivalent sites of peroxoΔ9D are the same as those of MMOH compound P and the (μ-1,2-peroxo)bis(μ-carboxylato) diiron model complex synthesized by Kim and Lippard [$\delta = 0.66$ mm/s (*36*)]; all of these δ values are slightly larger than the δ value observed for D84E RNR R2.

Low-temperature MCD/CD studies by Yang et al. suggest that both diferrous clusters of the complex of 18:0-ACP and $4e^-$ Δ9D have one four- and one five-coordinate iron site (*13*). Because the resonance Raman spectra of peroxoΔ9D are consistent with a symmetric μ-1,2-peroxo structure (*18*), it is tempting to speculate that peroxide occupies one open position at each iron site, giving rise to peroxodiferric clusters having one five- and one six-coordinate site. This could explain the observation of inequivalent sites in the Mössbauer spectrum of peroxoΔ9D. However, it should be noted that the crystallographically characterized cis μ-1,2-peroxodiferric complex of Ookubo et al. (*37*) exhibits two similar six-coordinate high-spin ferric sites (with the same N_3O_3 ligand set) and a Mössbauer spectrum consisting of two inequivalent doublets: $\delta(1) = 0.58$ mm/s, and $\Delta E_Q(1) = 0.74$ mm/s; $\delta(2) = 0.65$ mm/s, and $\Delta E_Q(2) = 1.7$ mm/s; in this case, the inequivalence is likely caused by the coordination of one O atom of the peroxo bridge trans to an imidazole ligand and the coordination of the other O atom of the peroxo bridge trans to an amine ligand.

While four peroxodiiron complexes that have been studied have yielded (average) isomer shifts that are larger than those of ferric non-peroxo complexes (*36*, *37*, *39*), two complexes provide an exception. A compound synthesized by Ménage et al. (*40*) exhibits one doublet: $\delta = 0.52$ mm/s, and $\Delta E_Q = 0.72$ mm/s; however, the O−O stretching frequencies are similar to those reported for the other peroxo complexes. Two distinct quadrupole doublets with an average δ of 0.55 mm/s [$\delta(1) = 0.47$ mm/s, and $\Delta E_Q(1) = 1.88$ mm/s; $\delta(2) = 0.63$ mm/s, and $\Delta E_Q(2) = 1.20$ mm/s] were also observed in the peroxo complex derived from the tetracarboxylate and pyridine-ligated diferrous complex studied by LeCloux et al. (*41*).

Finally, we comment on one other aspect of the peroxoΔ9D Mössbauer spectra. Our Mössbauer studies (*32*) have shown that resting Δ9D has a heterogeneous distribution of (diamagnetic) diiron clusters as indicated by the observation of quadrupole doublets belonging to three different species (Table 2). This distribution likely involves a mixture of oxo- and hydroxo-bridged clusters and perhaps clusters with other changes in the ligand environment. Such a heterogeneity is not restricted to Δ9D (*42*), and we suppose that it reflects the flexible coordination environment present in diiron enzymes. Interestingly, both peroxoΔ9D and peroxo-cycled Δ9D are spectroscopically rather homogeneous, suggesting that the initial heterogeneous environment is transformed into a homogeneous coordination upon complexation with 18:0-ACP and reaction with O_2.

Optical Properties of PeroxoΔ9D. The peroxodiiron complexes observed in both enzymes and model complexes have similar optical spectra, with a broad band extending from 500 to 1000 nm and an absorption maximum ranging from 600 to 725 nm. The ϵ value for peroxoΔ9D is comparable to that reported for ferritin [$\epsilon = 1000$ M^{-1} cm^{-1} (*19*)] but ~3.5-fold lower than that reported for $Fe(O_2)(OBz)_2[HB(pz')_3]_2$ [$\epsilon \sim 3800$ M^{-1} cm^{-1} (*43*)]. The large variability in the ϵ values for these related peroxo complexes may arise from the sensitivity of the peroxo → Fe^{3+} charge-transfer transitions to differences in the environment of the enzyme active site or various organic solvents (*39*). The ϵ value determined here for peroxoΔ9D by quantitation of diiron cluster intermediates closely matches that determined previously from the stoichiometry of 18:0-ACP titrations [$\epsilon_{700} = 1200 \pm 50$ M^{-1} cm^{-1} (*18*)]. This close match corroborates the accuracy of the different quantitation methods as well as the binding stoichiometry of 1 mol of 18:0-ACP per subunit of $4e^-$ Δ9D. Peroxo-cycled Δ9D was found to have a higher ϵ value at 340 nm per diiron cluster than resting Δ9D [$\epsilon_{340} = 4200$ M^{-1} cm^{-1} (*31*)]. This difference may originate from the variable amounts of oxo- and hydroxo-bridged clusters present in resting Δ9D as deduced from EXAFS and Mössbauer studies (*32*), while the oxo-bridged form may predominate in peroxo-cycled Δ9D.

Photolysis Experiments. The Mössbauer-detected photolysis of peroxoΔ9D at 4.2 K, leading to the appearance of a diferrous cluster and the reformation of the peroxo complex upon warming to 77 K, constitutes the first demonstration

of reversible O_2 adduct formation in a diiron enzyme. The photolysis result suggests that the 700 nm peroxo → Fe^{3+} charge-transfer transition involves an excited state in which the ready dissociation of O_2 is possible [an in-depth discussion of the electronic structure of peroxodiiron complexes has been published by Brunold et al. (*43*)]. The observation that peroxoΔ9D is quantitatively restored within 30 min at 77 K further shows that O_2 is effectively sequestered within the enzyme active site. Inspection of Table 2 shows that the diferrous state attained by photolysis has an average isomer shift (δ_{ave} = 1.22 mm/s) that is noticeably smaller than that of the $4e^-$ Δ9D·18:0 ACP complex (δ_{ave} = 1.27 mm/s), suggesting that the cluster observed at 4.2 K after photolysis resides in a constrained protein conformation. Similar observations have been reported, for instance, for myoglobin after low-temperature CO or O_2 photolysis (*44*).

Reactivity of PeroxoΔ9D. The study presented here has shown that all clusters in the $4e^-$ Δ9D sample are converted to peroxoΔ9D. We have previously shown that neither product nor H_2O_2 is released during decay of peroxoΔ9D and that both peroxoΔ9D and peroxo-cycled Δ9D retain full desaturase activity when added to assays containing the biological electron-transfer chain (*18*). Thus, the information presently available emphasizes the importance of redox transformations, substrate binding interactions (*48*), and cluster ligand conformations in controlling the outcome of Δ9D reactions. Moreover, for the experiments described here, the $4e^-$ Δ9D samples do not contain reducing equivalents other than those stored in the diferrous clusters. This suggests that the additional two electrons required to produce 2 mol of H_2O (or 1 mol of H_2O plus one oxo-bridged diferric cluster) per mole of O_2 consumed must come from a dinuclear cluster. Perhaps the oxidase reaction involves the release of O_2 from one diiron cluster to generate a diferrous cluster that could transfer the required two electrons, most likely by intramolecular transfer, to the other peroxo-bound center. This mechanism would imply the release of 1 mol of O_2 from peroxoΔ9D as suggested by the photolysis experiments. With our ability to generate quantitative preparations of peroxoΔ9D established, this possibility, and others, for the oxidase reaction mechanism is now experimentally testable.

REFERENCES

1. Fox, B. G. (1997) in *Comprehensive Biological Catalysis* (Sinnott, M., Ed.) pp 261−348, Academic Press, London.
2. Kurtz, D. M., Jr. (1997) *J. Biol. Inorg. Chem. 2*, 159−167.
3. Andersson, M. E., Högbom, M., Rinaldo-Matthis, A., Andersson, K. K., Sjöberg, B.-M., and Nordlund, P. (1999) *J. Am. Chem. Soc. 121*, 2346−2352.
4. Wallar, B. J., and Lipscomb, J. D. (1996) *Chem. Rev. 96*, 2625−2657.
5. Shanklin, J., and Cahoon, E. B. (1998) *Annu. Rev. Plant Physiol. Plant Mol. Biol. 49*, 611−641.
6. Harrison, P., and Arosio, P. (1996) *Biochim. Biophys. Acta 1275*, 161−203.
7. Elango, N., Radhakrishnan, R., Froland, W. A., Wallar, B. J., Earhart, C. A., Lipscomb, J. D., and Ohlendorf, D. H. (1997) *Protein Sci. 6*, 556−568.
8. Rosenzweig, A. C., Nordlund, P., Takahara, P. M., Frederick, C. A., and Lippard, S. J. (1995) *Chem. Biol. 2*, 409−418.
9. Fox, B. G., Hendrich, M. P., Surerus, K. K., Andersson, K. K., Froland, W. A., Lipscomb, J. D., and Münck, E. (1993) *J. Am. Chem. Soc. 115*, 3688−3701.
10. Lynch, J. B., Juarez-Garcia, C., Münck, E., and Que, L., Jr. (1989) *J. Biol. Chem. 264*, 8091−8096.
11. Hendrich, M. P., Münck, E., Fox, B. G., and Lipscomb, J. D. (1990) *J. Am. Chem. Soc. 112*, 5861−5865.
12. Hoffman, B. M., Sturgeon, B. E., Doan, P. E., DeRose, V. J., Liu, K. E., and Lippard, S. J. (1994) *J. Am. Chem. Soc. 116*, 6023−6024.
13. Yang, Y.-S., Broadwater, J. A., Fox, B. G., and Solomon, E. I. (1999) *J. Am. Chem. Soc. 121*, 2770−2783.
14. Pulver, S., Froland, W. A., Fox, B. G., Lipscomb, J. D., and Solomon, E. I. (1993) *J. Am. Chem. Soc. 115*, 12409−12422.
15. Pulver, S. C., Tong, W. H., Bollinger, J. M., Stubbe, J., and Solomon, E. I. (1995) *J. Am. Chem. Soc. 117*, 12664−12678.
16. Logan, D. T., Su, X.-D., Åberg, A., Regnström, K., Hajdu, J., Eklund, H., and Nordlund, P. (1996) *Structure 4*, 1053−1064.
17. Bollinger, J. M., Jr., Krebs, C., Vicol, A., Chen, S., Ley, B. A., Edmondson, D. E., and Huynh, B. H. (1998) *J. Am. Chem. Soc. 120*, 1094−1095.
18. Broadwater, J. A., Ai, J., Loehr, T. M., Sanders-Loehr, J., and Fox, B. G. (1998) *Biochemistry 37*, 14664−14671.
19. Pereira, A. S., Small, W., Krebs, C., Tavares, P., Edmondson, D. E., Theil, E. C., and Huynh, B. H. (1998) *Biochemistry 37*, 9871−9876.
20. Moënne-Loccoz, P., Baldwin, J., Ley, B. A., Loehr, T., and Bollinger, J. M., Jr. (1998) *Biochemistry 37*, 14659−14663.
21. Möenne-Loccoz, P., Krebs, K., Herlihy, K., Edmondson, D. E., Theil, E. C., Huynh, B. H., and Loehr, T. M. (1999) *Biochemistry 38*, 5290−5295.
22. Shu, L., Nesheim, J. C., Kauffmann, K., Münck, E., Lipscomb, J. D., and Que, L., Jr. (1997) *Science 275*, 515−518.
23. Liu, K. E., Valentine, A. M., Wang, D., Huynh, B. H., Edmondson, D. E., Salifoglou, A., and Lippard, S. J. (1995) *J. Am. Chem. Soc. 117*, 10174−10185.
24. Valentine, A. M., Stahl, S. S., and Lippard, S. J. (1999) *J. Am. Chem. Soc. 121*, 3867−3887.
25. Burdi, D., Sturgeon, B. E., Tong, W. H., Stubbe, J., and Hoffman, B. M. (1996) *J. Am. Chem. Soc. 118*, 281−282.
26. Sturgeon, B. E., Burdi, D., Chen, S., Huynh, B.-H., Edmondson, D. E., Stubbe, J., and Hoffman, B. M. (1996) *J. Am. Chem. Soc. 118*, 7551−7557.
27. Willems, J.-P., Lee, H.-I., Burdi, D., Doan, P. E., Stubbe, J., and Hoffman, B. M. (1997) *J. Am. Chem. Soc. 119*, 9816−9824.
28. Riggs-Gelasco, P. J., Shu, L., Chen, S., Burdi, D., Huynh, B. H., Que, L., Jr., and Stubbe, J. (1998) *J. Am. Chem. Soc. 120*, 849−860.
29. Lee, S.-K., Fox, B. G., Froland, W. F., Lipscomb, J. D., and Münck, E. (1993) *J. Am. Chem. Soc. 115*, 6450−6451.
30. Fox, B. G., Shanklin, J., Ai, J., Loehr, T. M., and Sanders-Loehr, J. (1994) *Biochemistry 33*, 12776−12786.
31. Fox, B. G., Shanklin, J., Somerville, C., and Münck, E. (1993) *Proc. Natl. Acad. Sci. U.S.A. 90*, 2486−2490.
32. Shu, L., Broadwater, J. A., Achim, C., Fox, B. G., Münck, E., and Que, L., Jr. (1998) *J. Biol. Inorg. Chem. 3*, 392−400.
33. Lindqvist, Y., Huang, W., Schneider, G., and Shanklin, J. (1996) *EMBO J. 15*, 4081−4092.
34. Hoffman, B. J., Broadwater, J. A., Johnson, P., Harper, J., Fox, B. G., and Kenealy, W. R. (1995) *Protein Expression Purif. 6*, 646−654.
35. Broadwater, J. A., and Fox, B. G. (1998) *Protein Expression Purif. 15*, 314−326.
36. Kim, K., and Lippard, S. J. (1996) *J. Am. Chem. Soc. 118*, 4914−4915.
37. Ookubo, T., Sugimoto, H., Nagayama, T., Masuda, H., Sato, T., Hayashi, Y., Uehara, A., and Suzuki, M. (1996) *J. Am. Chem. Soc. 118*, 701−702.
38. Dong, Y., Yan, S., Young, V. G., Jr., and Que, L., Jr. (1996) *Angew. Chem., Int. Ed. 35*, 618−620.
39. Dong, Y., Ménage, S., Brennan, B. A., Elgren, T. E., Jang, H. G., Pearce, L. L., and Que, L., Jr. (1993) *J. Am. Chem. Soc. 115*, 1851−1859.
40. Ménage, S., Brennan, B. A., Juarez-Garcia, C., Münck, E., and Que, L., Jr. (1990) *J. Am. Chem. Soc. 112*, 6423−6425.

41. LeCloux, D. D., Barrios, A. M., Mizoguchi, T. J., and Lippard, S. J. (1998) *J. Am. Chem. Soc. 120*, 9001−9014.
42. Shu, L., Liu, Y., Lipscomb, J. D., and Que, L., Jr. (1996) *J. Biol. Inorg. Chem. 1*, 297−304.
43. Brunold, T. C., Tamura, N., Kitajima, N., Moro-oka, Y., and Solomon, E. I. (1998) *J. Am. Chem. Soc. 120*, 5674−5690.
44. Frauenfelder, H., Parak, F., and Young, R. D. (1988) *Annu. Rev. Biophys. Biophys. Chem. 17*, 451−479.
45. Feig, A. L., Becker, M., Schindler, S., van Eldik, R., and Lippard, S. J. (1996) *Inorg. Chem. 35*, 2590−2601.
46. Petrou, T. L., Armstrong, F. A., Sykes, A. G., Harrington, P. C., and Wilkins, R. G. (1981) *Biochim. Biophys. Acta 670*, 377−384.
47. Nesheim, J. C., and Lipscomb, J. D. (1996) *Biochemistry 35*, 10240−10247.
48. Haas, J. A., and Fox, B. G. (1999) *Biochemistry* (in press).

BI9914199